



Power generation mechanism and performance analysis of parametrically excited piezoelectric composite devices for vibratory energy harvesting



Tianjun Yu^a, Sha Zhou^{b,*}

^a Key Laboratory of Dynamics and Control of Flight Vehicle, Ministry of Education and School of Aerospace Engineering, Beijing Institute of Technology, Beijing 100081, China

^b Department of Engineering Mechanics, Zhejiang University, Hangzhou 310027, China

ARTICLE INFO

Keywords:

Nonlinear energy harvesting
Piezoelectric composite structure
Electromechanical coupling
Energy conversion efficiency
Parametric resonance

ABSTRACT

Vibratory energy harvesting, that is, capturing the energy of environmental vibrations and transforming into electric forms, has flourished as an important research field for micro-power generation. As a means of mechanical amplification, a subtly designed parametrically excited energy harvester could produce more power output than a corresponding directly excited energy harvester. In this paper, a simple but effective composite structure for realizing parametrically excited piezoelectric energy harvesting is first introduced, and analyzed in details by combining the harmonic balance method and the energy balance equation. Direct numerical simulations are performed to validate the theoretical predictions. Special features describing two types of observable resonances are then revealed by comprehensively monitoring the frequency response of the mean-square voltage, the input power, the output power, the energy conversion efficiency, the phase angle and the phase difference. By comparing with the directly excited energy harvesters, the advantages of parametrically excited energy harvesters are finally revealed. The most important point view of this work is that the performance of vibratory energy harvesters stems from the input power. It is suggested that superior self-adjustable broadband vibration harvesting could be exploited by constructing optimal phase to maximize the input power to achieve supreme output power.

1. Introduction

Vibratory energy harvesting have received considerable attention in the literature recently, due to the fact that different vibration responses exist in various mechanical systems and human body systems, for instance, the whirling motion of rotors [1–6], the instability and resonant response of pipes conveying fluid [7–10], the flutter and dynamics of plates and wings [11–15], the heart pumping and the arterial pulse [16–19], etc. Vibration-based piezoelectric energy harvesters use the electromechanical coupling effect of piezoelectric crystals experiencing ambient vibrations to produce electric energy that can be simultaneously stored up for supplying power. In the past few years, there have been increasing interests on designing multifunctional structures by combining energy harvesting and vibration suppression [20–23].

For the vibratory energy harvesters operating based on the principle of linear resonance, the frequency bandwidth is usually very narrow, that limits the applicability and usefulness of the harvesters. Nonlinearities arising from the nonlinear strain-deflection relations

or nonlinear constitutive relations are inherently present in the vibratory energy harvesting systems. The introduction of nonlinearities into the innovative design of vibratory energy harvesters has been a widespread concerned topic [24,25]. Some results have pointed out that elaborately introduced nonlinearity could be beneficial to harvest energy because the harvester's operation bandwidth can be extended [26–31] when compared to the linear device.

There have been a tremendous amount of research dealing with the system modeling and performance optimization of harvesting energy via directly excited piezoelectric composite beam [32–40]. Such nonlinear energy harvesters take advantage of the forced resonance, which occurs from external forcing of the beam structure at its primary mode, subharmonic or superharmonic mode. It is worth noting that nonlinearity excited directly yields physically nonunique solutions of response for certain frequency domains which can be characterized by the presence of coexisting motions, and this type of nonlinear energy harvesters are not always guaranteed to hold the expected strong resonant state. Actually, the practical operating state is depending on the basin of attraction of the coexisting solutions [31,41]. In

* Corresponding author.

E-mail address: lilyzhou191@hotmail.com (S. Zhou).

order to achieve broadband performance, nonlinear energy harvesting in the fully developed turbulence is a potential scheme. That could be modeled as a directly excited electromechanical system under wide-band or narrowband noises, and the method of nonlinear stochastic can be applied to estimate the performance metrics.

In the last decade, energy harvesting through parametrically excited nonlinear piezoelectric beams, as a promising concept, emerged [42–48]. This type of nonlinear energy harvesters utilizes the parametric resonance to improve the harvester’s performance. By comparing with the energy harvesters under forced resonance, in this paper, it is concluded that the potential benefits of parametric resonance for harvesting energy are larger responses and wider bandwidths on input power and output power. In fact, a relatively small parametric modulation level may induce a dynamical instability when the modulation frequency is close to double of the mode frequency, and a wider response bandwidth could be obtained as increasing the strength of the parametric modulation.

To the best of our knowledge, no research has been conducted to systematically study the performance metrics of parametrically excited piezoelectric energy harvesters, including mean-square voltage output, input power, output power and energy conversion efficiency. In particular, there is still a lack of rational research on the crucial performance metric, efficiency (the ratio of the electrical power net output to the mechanical power net input). There are two main reasons resulting in incorrect estimation of efficiency, the erroneous definition on input power and inappropriate dimensionless governing equations employed. More importantly, the input power, as the basis of efficiency analysis, could also interpret the power generation mechanism. For the directly excited piezoelectric energy harvesters [49], the input mechanical power, actually, is influenced by the phase difference between the dynamical response and the deterministic excitation, and the corresponding conclusions can be degenerated to these of the purely mechanical systems [50] when the electromechanical coupling factor is set to zero.

Recently, we find that by employing the energy balance equation of electromechanical coupling system, mathematical expressions on the input mechanical power and the output electrical power can be generated naturally and new set of dimensionless transformations can capture two-way coupling effects, thus, rational efficiency research has been achieved for the energy harvesters under random excitations [51,52]. It is noteworthy that the concept of energy balance [53], as a universal law in physics, could be not only applied to efficiency analysis of the electromechanical coupling systems under random excitations, but also to power generation mechanism analysis of the electromechanical coupling system under deterministic excitations. Galloping or flutter-based nonlinear energy harvesting has also received increasing attention. The response of such self-excited dynamical system is actually a stability issue, and in the governing equation the excitation source is characterized by an autonomous term with respect to the flow velocity. Due to the interactive effect between the fluid motion and the small mechanical disturbance, the mechanical system could capture kinetic energy from the fluid system when the flow velocity exceeds the critical threshold, meanwhile, a steady-state mechanical response with finite amplitude is triggered and the input energy is generated, thus, the output energy can be produced via electromechanical coupling effect. The comparison on the energy conversion efficiency of the same harvesting system under self-excitation, direct excitation and parametric excitation is also an important research topic, in which the establishment of the energy balance equation will be a crucial link.

This paper addresses critical issues related to power generation mechanism and comprehensive performance analysis of the parametrically excited piezoelectric energy harvesters. The rest of this paper is organized as follows: In Section 2, a parametrically excited nonlinear energy harvester is first introduced and its electromechanical coupling equations are then nondimensionalized by using a new set of dimen-

sionless transformations. In Section 3, mean-square voltage in the steady-state are obtained by employing the harmonic balance method and its dependency relationships on system parameters are analyzed. In Section 4, explicit expressions on input power, output power and efficiency are then derived by means of energy balance equation and then the variation law of performance metrics with system parameters is investigated in detail. In Section 5, by comparing with the directly excited energy harvesters, the advantages of parametrically excited energy harvesters are finally revealed. In Section 6, we end the paper with concluding remarks.

2. Electromechanical composite structure

Considering a parametrically excited piezoelectric device with von Karman geometric nonlinearity, realized by a composite structure including three components, that is, outer sleeve, piezoelectric beam and inner sleeve, as shown in Fig. 1(a). The proposed composite structure is simple, with minimum number of components, and is encapsulated as a whole, so it can withstand multiple loads of outdoor complex and harsh environments, and avoid the direct damage of rain and snow to the internal electromechanical coupling system. Based on the

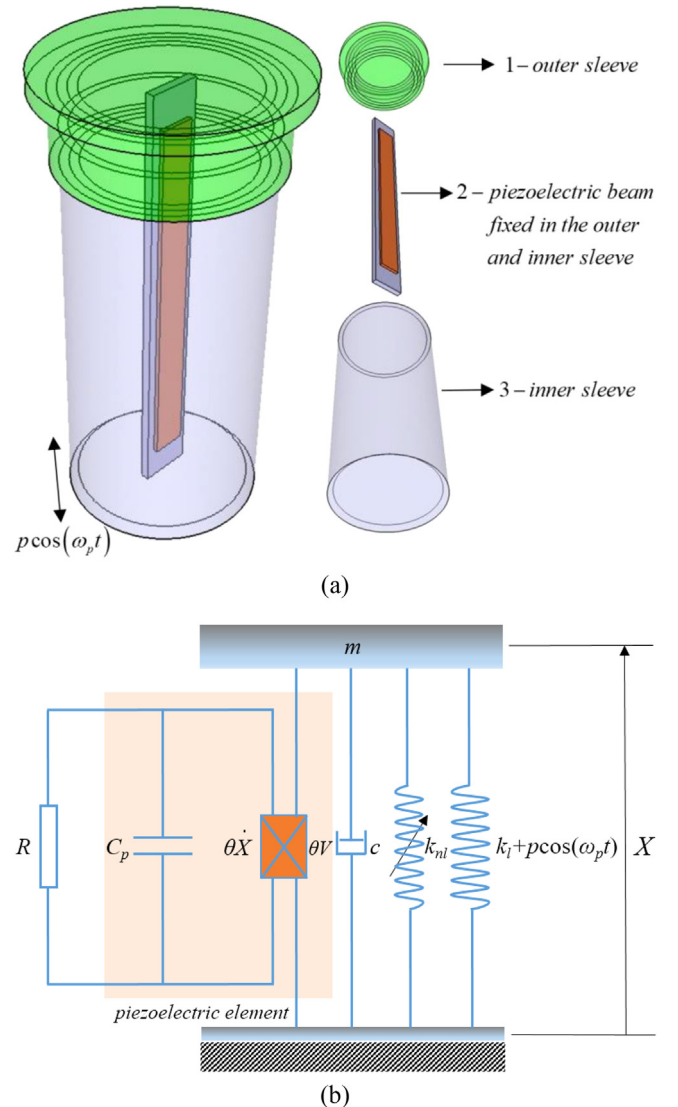


Fig. 1. A parametrically excited piezoelectric energy harvester. (a) Continuum model; (b) Lumped-parameter model.

extended Hamilton's principle with internal electrical energy and a single-mode truncation of the beam dynamics, a lumped-parameter model can be established (Fig. 1 (b)) and the electromechanical coupling governing equations are obtained as follows

$$m\ddot{X} + c\dot{X} + k_l X + k_{nl} X^3 - \theta V + pX \cos(\omega_p t) = 0 \quad (1a)$$

$$C_p \dot{V} + \frac{1}{R} V + \theta \dot{X} = 0 \quad (1b)$$

where the overdot represents the derivative with respect to time t . X and V denotes the displacement response of the beam and the voltage response measured across the equivalent resistance R , respectively. c is the mechanical damping, θ is the electromechanical coupling, C_p is the capacitance. k_l and k_{nl} is linear and nonlinear stiffness, respectively. p and ω_p represents the amplitude and the frequency of the parametric excitation, respectively.

Introducing the dimensionless variables and parameters as follows

$$\bar{X} = \frac{X}{l}, \bar{V} = V \sqrt{\frac{C_p}{l^2 k_l}}, \tau = \frac{t}{T} = t \omega_0 = t \sqrt{\frac{k_l}{m}}, \Omega = \frac{\omega_p}{\omega_0}$$

$$\mu = \frac{c}{m \omega_0}, \alpha = \frac{k_{nl} l^2}{k_l}, \chi = \frac{\theta}{\sqrt{k_l C_p}}, \beta = \frac{1}{\omega_0 R C_p}, f = \frac{p}{m \omega_0^2} \quad (2)$$

Eq. (1) becomes, after dropping all overbars for convenience

$$X'' + \mu X' + X + \alpha X^3 - \chi V + f X \cos(\Omega \tau) = 0 \quad (3a)$$

$$V' + \beta V + \chi X' = 0 \quad (3b)$$

where the prime represents the differential with respect to the dimensionless time τ , μ is the dimensionless mechanical damping, α is the dimensionless nonlinearity coefficient, χ denote the dimensionless electromechanical coupling, β is the time constant. f and Ω is the dimensionless excitation amplitude and frequency, respectively. It is noteworthy that we construct a new set of dimensionless transformation (2) to derive a reasonable dimensionless electromechanical coupling model which can capture the two-way coupling characteristics. Thus, the inconsistency of the analysis results of energy conversion efficiency based on the original equations and the dimensionless equations can be avoided.

3. Steady-state solutions

In this section, approximate analytic solutions to periodic steady-state response of the parametrically excited nonlinear piezoelectric energy harvester described by system (3) are presented. Apart from the subharmonic parametric resonance, primary parametric resonance is also considered as potential for vibration energy harvesting when excitation amplitude level is relatively high. Since the coefficients of the nonlinear terms, in general, are decided by the geometrical and physical parameters of specific structure and which mode is involved, thus, for a certain structure excited by stationary frequency, although the coefficients of the nonlinear terms are constant, as excitation level is increased, the nonlinear effects still significantly grow and more harmonic components should be taken into account to predict the dynamic behaviors accurately. In order to ensure the accuracy of harmonic balance method, in this work, second-order approximation to the steady-state solution of the electromechanical coupling system is employed. A reasonably small damping coefficient ($\mu = 0.02$) and a relatively moderate excitation amplitude ($f = 0.4$) is used, to simultaneously capture the primary and subharmonic parametric resonance in one frequency sweep. The results of the response behaviors of the harvester under two type of parametric resonances are examined by using mean-square voltage output at different parametric excitation frequencies as a performance metric.

3.1. Primary parametric resonance

When the excitation frequency Ω is in the vicinity of the natural frequency ω , i.e. $\Omega \approx \omega$, primary parametric resonance may arise, approximate solutions of Eq. (3) in this case, take the form

$$X = A_1 \cos(\Omega \tau) + A_2 \sin(\Omega \tau) + A_3 \cos(2\Omega \tau) + A_4 \sin(2\Omega \tau) + A_5$$

$$V = A_6 \cos(\Omega \tau) + A_7 \sin(\Omega \tau) + A_8 \cos(2\Omega \tau) + A_9 \sin(2\Omega \tau) \quad (4)$$

where A_i ($i = 1, 2, \dots, 9$) represents the steady-state response amplitude to be determined. Inserting Eq. (4) into Eq. (3) and equating coefficients of the zeroth-order harmonic, first-order harmonic and second-order harmonic, respectively, one obtains the following coupled nonlinear algebraic equations for A_i

$$K_A A = N L_A \quad (5)$$

where

$$A = [A_1 \ A_2 \ A_3 \ A_4 \ A_5 \ A_6 \ A_7 \ A_8 \ A_9]^T$$

and

$$K_A = \begin{bmatrix} 1 - \Omega^2 & \Omega \mu & \frac{f}{2} & 0 & f_0 & \chi & 0 & 0 & 0 \\ -\Omega \mu & 1 - \Omega^2 & 0 & \frac{f}{2} & 0 & 0 & \chi & 0 & 0 \\ \frac{f}{2} & 0 & 1 - 4\Omega^2 & 2\Omega \mu & 0 & 0 & 0 & \chi & 0 \\ 0 & \frac{f}{2} & -2\Omega \mu & 1 - 4\Omega^2 & 0 & 0 & 0 & 0 & \chi \\ \frac{f}{2} & 0 & 0 & 0 & 1 & 0 & 0 & 0 & 0 \\ 0 & -\Omega \chi & 0 & 0 & 0 & \beta & \Omega & 0 & 0 \\ \Omega \chi & 0 & 0 & 0 & 0 & 0 & -\Omega & \beta & 0 \\ 0 & 0 & 0 & -2\Omega \chi & 0 & 0 & 0 & \beta & 2\Omega \\ 0 & 0 & 2\Omega \chi & 0 & 0 & 0 & 0 & -2\Omega & \beta \end{bmatrix}$$

and

$$N L_A = \begin{bmatrix} \frac{3\alpha}{4} (A_1^2 + A_2^2 + 2A_3^2 + 2A_4^2 + 4A_5^2 + 4A_3 A_5) A_1 + 3\alpha A_2 A_4 A_5 \\ \frac{3\alpha}{4} (A_1^2 + A_2^2 + 2A_3^2 + 2A_4^2 + 4A_5^2 - 4A_3 A_5) A_2 + 3\alpha A_1 A_4 A_5 \\ \frac{3\alpha}{4} (2A_1^2 + 2A_2^2 + A_3^2 + A_4^2 + 4A_5^2) A_3 + \frac{3\alpha}{2} (A_1^2 - A_2^2) A_5 \\ \frac{3\alpha}{4} (2A_1^2 + 2A_2^2 + A_3^2 + A_4^2 + 4A_5^2) A_4 + 3\alpha A_1 A_2 A_5 \\ \frac{3\alpha}{2} (A_1^2 + A_2^2 + A_3^2 + A_4^2) A_5 + \alpha A_3^3 + \frac{3\alpha}{2} A_1 A_2 A_4 + \frac{3\alpha}{4} (A_1^2 - A_2^2) A_3 \\ 0 \\ 0 \\ 0 \\ 0 \end{bmatrix} \quad (6)$$

Unknown coefficients in A can be found by solving the nonlinear algebraic Eq. (5) in terms of Newton-Raphson method. Further, the mean-square voltage of system (3) in the case of primary parametric resonance can be evaluated as

$$E[V^2]_{PPR} = \frac{\Omega}{2\pi} \int_0^{\frac{2\pi}{\Omega}} V^2 d\tau = \frac{1}{2} (A_6^2 + A_7^2 + A_8^2 + A_9^2) \quad (7)$$

In order to compare the analytical and numerical results quantitatively, Fig. 2 shows variation of the mean-square voltage output with the excitation frequency in the vicinity of the primary parametric resonance obtained by numerical simulation (NS) and harmonic balance method (HBM), respectively. Such frequency response as a critical performance metric is created by quasi-statically varying the parametric excitation frequency and then recording the steady-state response of mean-square voltage at each frequency. The most beneficial merit of the frequency response is that effective bandwidth and possible jumping behaviors depending on specific applications can be evidently observed. By comparing the overlap between the numerical results and the analytic one, we verify the validity of the harmonic balance method with second-order approximation for the estimation of frequency response. It is inspiring to see that the analytic solution is slightly smaller than that of the numerical simulation and the peak error for the forward frequency sweep is limited within 4%. Physical explanation is that the system described by limited harmonic compo-

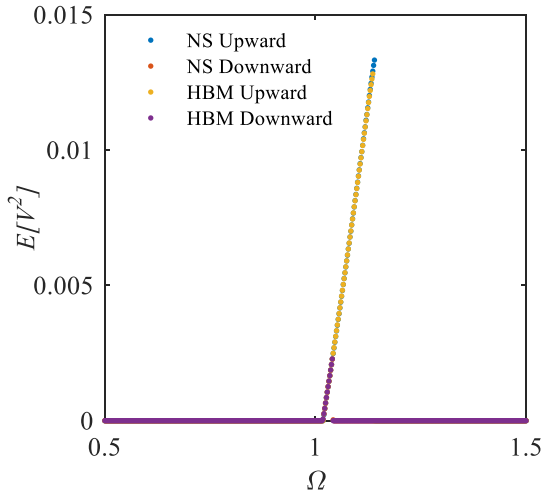


Fig. 2. Mean-square voltage response in frequency domain for primary parametric resonance. $\alpha = 1, \beta = 0.1, \chi = 0.3, \mu = 0.02, f = 0.4$.

nents is actually equivalent to another system with higher stiffness, consequently, the deflection amplitude of the corresponding mechanical structure and voltage response is decreased, compared with the original system.

3.2. Subharmonic parametric resonance

When Ω is in the vicinity of 2ω , subharmonic parametric resonance may arise, approximate solutions of Eq. (3) in this case, take the form

$$X = B_1 \cos\left(\frac{1}{2}\Omega\tau\right) + B_2 \sin\left(\frac{1}{2}\Omega\tau\right) + B_3 \cos\left(\frac{3}{2}\Omega\tau\right) + B_4 \sin\left(\frac{3}{2}\Omega\tau\right)$$

$$V = B_5 \cos\left(\frac{1}{2}\Omega\tau\right) + B_6 \sin\left(\frac{1}{2}\Omega\tau\right) + B_7 \cos\left(\frac{3}{2}\Omega\tau\right) + B_8 \sin\left(\frac{3}{2}\Omega\tau\right) \quad (8)$$

where B_i ($i = 1, 2, \dots, 8$) represents the steady-state response amplitude to be determined. Inserting Eq. (8) into Eq. (3) and performing the same procedure followed previously, one obtains the following coupled nonlinear algebraic equations for B_i

$$\mathbf{K}_B \mathbf{B} = \mathbf{NL}_B \quad (9)$$

where $\mathbf{B} = [B_1 \ B_2 \ B_3 \ B_4 \ B_5 \ B_6 \ B_7 \ B_8]^T$ and

$$\mathbf{K}_B = \begin{bmatrix} 1 - \frac{\Omega^2}{4} + \frac{f}{2} & \frac{\Omega\mu}{2} & \frac{f}{2} & 0 & \chi & 0 & 0 & 0 \\ -\frac{\Omega\mu}{2} & 1 - \frac{\Omega^2}{4} - \frac{f}{2} & 0 & \frac{f}{2} & 0 & \chi & 0 & 0 \\ \frac{f}{2} & 0 & 1 - \frac{9\Omega^2}{4} & \frac{3\Omega\mu}{2} & 0 & 0 & \chi & 0 \\ 0 & \frac{f}{2} & -\frac{3\Omega\mu}{2} & 1 - \frac{9\Omega^2}{4} & 0 & 0 & 0 & \chi \\ 0 & -\frac{\Omega\chi}{2} & 0 & 0 & \beta & \frac{\Omega}{2} & 0 & 0 \\ \frac{\Omega\chi}{2} & 0 & 0 & 0 & -\frac{\Omega}{2} & \beta & 0 & 0 \\ 0 & 0 & 0 & -\frac{3\Omega\chi}{2} & 0 & 0 & \beta & \frac{3\Omega}{2} \\ 0 & 0 & \frac{3\Omega\chi}{2} & 0 & 0 & 0 & -\frac{3\Omega}{2} & \beta \end{bmatrix}$$

and

$$\mathbf{NL}_B = \begin{bmatrix} \frac{3\alpha}{4}(B_1^2 + B_2^2 + 2B_3^2 + 2B_4^2 + B_1B_3 + 2B_2B_4)B_1 - \frac{3\alpha}{4}B_2^2B_3 \\ \frac{3\alpha}{4}(B_1^2 + B_2^2 + 2B_3^2 + 2B_4^2 - 2B_1B_3 - B_2B_4)B_2 + \frac{3\alpha}{4}B_1^2B_4 \\ \frac{3\alpha}{4}(2B_1^2 + 2B_2^2 + B_3^2 + B_4^2)B_3 + \frac{\alpha}{4}(B_1^2 - 3B_2^2)B_1 \\ \frac{3\alpha}{4}(2B_1^2 + 2B_2^2 + B_3^2 + B_4^2)B_4 + \frac{\alpha}{4}(3B_1^2 - B_2^2)B_2 \\ 0 \\ 0 \\ 0 \\ 0 \end{bmatrix} \quad (10)$$

Then, similarly, the nonlinear algebraic Eq. (9) is solved iteratively to define the mean-square voltage of system (3) in the case of subharmonic parametric resonance

$$E[V^2]_{SPR} = \frac{\Omega}{2\pi} \int_0^{\frac{2\pi}{\Omega}} v^2 d\tau = \frac{1}{2} (B_5^2 + B_6^2 + B_7^2 + B_8^2) \quad (11)$$

The frequency–response results in Fig. 3 are obtained by numerical simulation and the harmonic balance method with second-order approximation, respectively. Obviously, the subharmonic parametric resonance trigger much larger response and the frequency range of mean-square voltage response is much wider than the primary parametric resonance when other system parameters are fixed. Due to the superior performance resulting from forward frequency sweep, it is expectable that the parametrically excited piezoelectric energy harvester is more suited to the ambient environment with slow varying broadband frequency and relatively high excitation level. The comparison result shows that the second-order harmonic balance produces fairly accurate solutions to this type of electromechanical coupling systems.

3.3. The effect of parameters on steady-state solutions

The dependence of mean-square voltage on the dimensionless system parameters based on the approximate analytic solutions obtained in Section 3.1 and 3.2 are now examined. Since the analytic results are in good agreement with the numerical results, hereafter, only harmonic balance results with two-terms approximation are shown.

We first study the effect of nonlinear coefficient α on the mean-square voltage. Four values are considered for α and mean-square voltage frequency response are together plotted in Fig. 4. For both primary and subharmonic parametric resonance, the results indicate that α is inverse proportional to the magnitude of the mean-square voltage, that is, decreasing α gives rise to higher output voltage as a result of stronger amplitude response induced by easily available parametric instability. Moreover, the bandwidth of the voltage response appears to be independent with α . Therefore, one could expect that these properties may be very helpful for harvesting energy in the presence of inherent weak nonlinearity. In addition, it is noteworthy that the response of the subharmonic parametric resonance extends over a broad frequency range and the peak is naturally high, while the bandwidth of the primary parametric resonance is relatively much narrow, accompanied with much low peak.

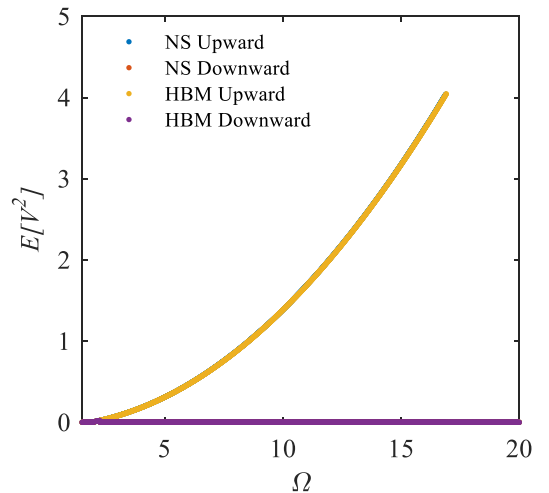


Fig. 3. Mean-square voltage response in frequency domain for subharmonic parametric resonance. $\alpha = 1, \beta = 0.1, \chi = 0.3, \mu = 0.02, f = 0.4$.

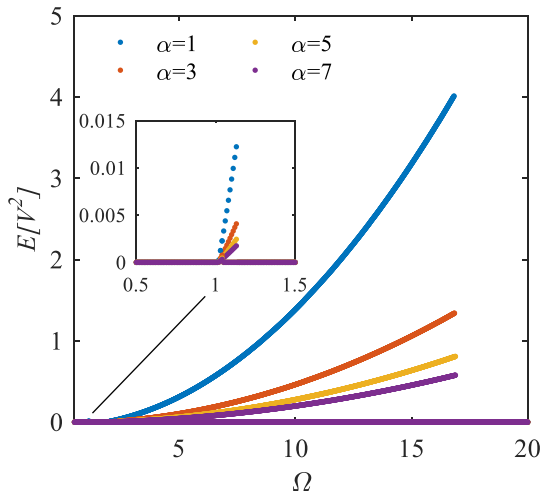


Fig. 4. Variation of mean-square voltage with α . $f = 0.4$, $\beta = 0.1$, $\mu = 0.02$, $\chi = 0.3$.

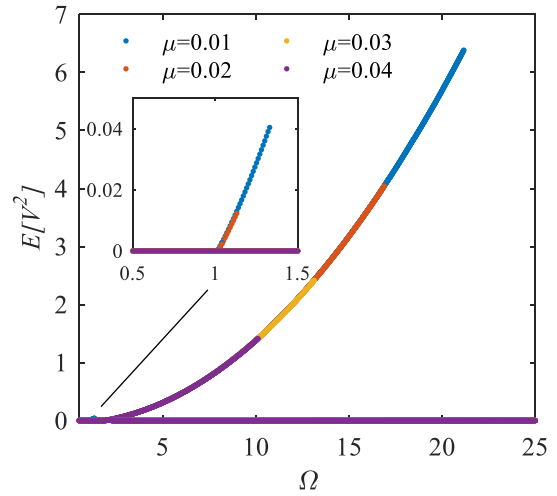


Fig. 6. Variation of mean-square voltage with μ . $f = 0.4$, $\beta = 0.1$, $\alpha = 1$, $\chi = 0.3$.

We then survey the effect of excitation amplitude, f , on the mean-square voltage, as shown in Fig. 5. As the excitation amplitude is decreased from 0.6 to 0.3, the mean-square voltage drops significantly for both primary and subharmonic parametric resonance. Especially for the primary parametric resonance, when f is less than or equal to 0.3, the voltage response ceases to exist and vibration energy cannot be harvested. In fact, same phenomenon can be also observed for the subharmonic parametric resonance just corresponding to a much smaller excitation amplitude. In other words, excitation amplitude's minimum should be maintained for harvesting energy by using parametric resonance. On the other hand, as the excitation amplitude is decreased, the frequency range wherein parametric instability occurs and steady-state voltage response forms shrinks evidently. These properties indicate that better performance would be expected with stronger excitation.

Figure 6 shows that the mean-square voltage for both primary and subharmonic parametric resonance drop rapidly and the bandwidth shrinks significantly as mechanical damping μ is increased. When excitation amplitude is fixed, relatively high damping which is above a certain threshold can actually prevent the occurrence of parametric instability and it will be detrimental to harvesting energy. This phe-

nomenon first arises in the frequency range of the primary parametric resonance and then the subharmonic parametric resonance. By synthesizing Fig. 5 and Fig. 6, one could conclude that it is allowed with higher damping and weaker excitation to establish subharmonic parametric resonance and wider applications can be expected.

Figure 7 demonstrates the effect of time constant β on the mean-square voltage. The results show that the mean-square voltage reaches maximum in the open-circuit scenario, and the frequency range of voltage response shrinks as β is increased from zero. It is noted that the response of primary parametric resonance is more sensitive to the increased β than that of the subharmonic resonance. The parametric instability settles down with higher time constant.

Figure 8 shows the influence of electromechanical coupling χ on the mean-square voltage. For both primary and subharmonic parametric resonance, optimum mean-square voltage exists. This can be explained that, for given other system parameters, the voltage response is actually affected by two factors, that is, deflection amplitude of the mechanical structure and electromechanical coupling χ . As χ is increased, electromechanical coupling induces a partial energy migration to the electrical system, captured by load resistance. This leads the deflection amplitude to decrease with χ . As a result, an opti-

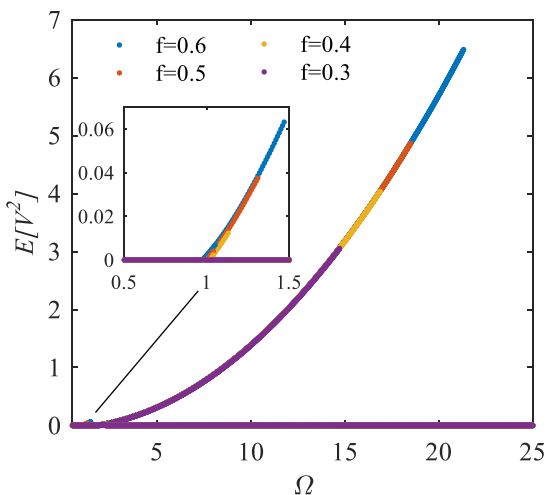


Fig. 5. Variation of mean-square voltage with f . $\mu = 0.02$, $\alpha = 1$, $\beta = 0.1$, $\chi = 0.3$.

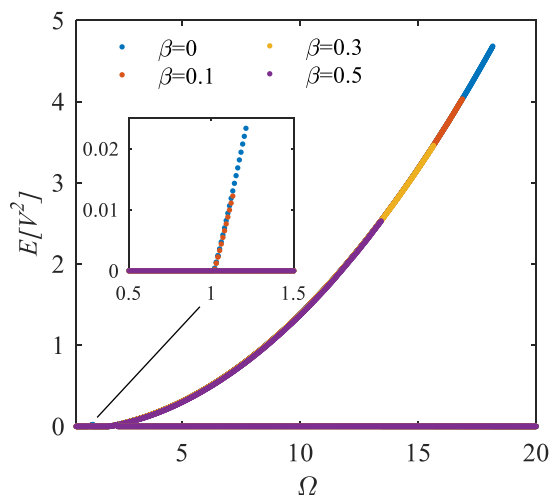


Fig. 7. Variation of mean-square voltage with β . $f = 0.4$, $\mu = 0.02$, $\alpha = 1$, $\chi = 0.3$.

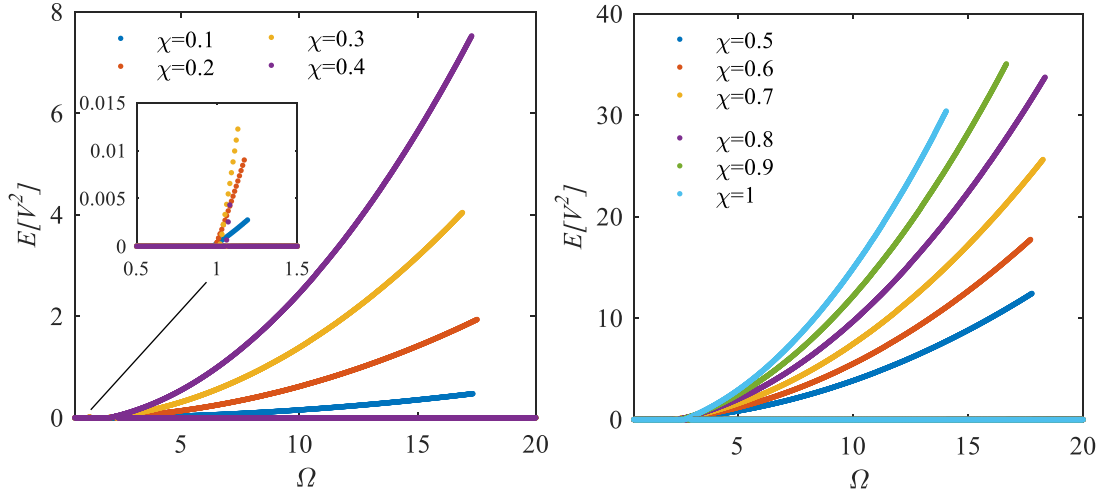


Fig. 8. Variation of mean-square voltage with χ . $f = 0.4$, $\mu = 0.02$, $\alpha = 1$, $\beta = 0.1$.

mal χ exists at which the generated voltage is maximized. For the primary parametric resonance, when χ is greater than or equal to 0.5, the voltage response ceases to exist and vibration energy cannot be harvested. It is also evident that the primary parametric resonance requires a smaller coupling value to stay the best performance than the subharmonic parametric resonance. It is noteworthy that the bandwidth shrinks significantly near the region where the optimal χ is located.

4. Energy conversion efficiency and work done on parametric excitation

In this section, the energy conversion efficiency of parametrically excited piezoelectric energy harvester (3) is analyzed via the mean power balance equation as

$$\frac{dE[H]}{dt} = -\mu E[X^2] + \chi E[X'V] - fE[XX'\cos\Omega\tau] \quad (12)$$

where H represents the conservative energy corresponding to the mechanical system, $H(X, X') = X^2/2 + X'^2/2 + \alpha X^4/4$, and $E[\cdot]$ denotes the averaging operator, that is, $E[\cdot] = \frac{1}{T_1} \int_0^{T_1} (\cdot) d\tau$, herein, T_1 represents the corresponding period.

Note that Eq. (12) can be easily derived by taking the time derivative of H , making use of the electromechanical coupling governing equation (3) and then averaging. Such mean power balance equation contains useful information on power input, power output, and power dissipation. To be specific, $\mu E[X^2]$ represents the power dissipated by mechanical damping, $\chi E[X'V]$ is the power transferred from the mechanical system to the electric system, which is equal to $\beta E[V^2]$, the net output power, and $-fE[XX'\cos\Omega\tau]$ is the net input power supplied by parametric excitation.

For the primary parametric resonance, taking into account the periodic solution expressed in Eq. (4), the input power can then be written as

$$E[P_{in}]_{PPR} = \frac{1}{4} \Omega f \sqrt{A_1^2 + A_2^2} \left[2A_5 \sin\phi_1 + \sqrt{A_3^2 + A_4^2} \sin(\phi_2 - \phi_1) \right] \quad (13)$$

where A_5 is negative based on the system parameters selected in this paper and the phase angles describing the first-order harmonic and the second-order harmonic motion of the mechanical system are

$$\phi_1 = \arctan\left(-\frac{A_2}{A_1}\right), \phi_2 = \arctan\left(-\frac{A_4}{A_3}\right) \quad (14)$$

It is noteworthy that the net input power is proportional to the excitation frequency and amplitude, and directly related to the amplitude, the phase angle and the phase difference of the response. The first term in Eq. (13) represents the contribution of the first-order harmonic coupled with zeroth-order harmonic, which is the primary source of net power inflow from the outside excitation into the energy harvesting system, and the second term in Eq. (13) represents the contribution of the second-order harmonic, which is the secondary source of net power inflow from the outside excitation into the energy harvesting system.

Hence, the efficiency for the primary parametric resonance can be expressed as

$$\eta_{PPR} = \frac{E[P_{out}]_{PPR}}{E[P_{in}]_{PPR}} = \frac{2\beta(A_6^2 + A_7^2 + A_8^2 + A_9^2)}{\Omega f \sqrt{A_1^2 + A_2^2} \left[2A_5 \sin\phi_1 + \sqrt{A_3^2 + A_4^2} \sin(\phi_2 - \phi_1) \right]} \quad (15)$$

Similarly, for the subharmonic parametric resonance, taking into account the periodic solution expressed in Eq. (8), the input power is written as

$$E[P_{in}]_{SPR} = \frac{1}{8} \Omega f \times \sqrt{B_1^2 + B_2^2} \left[\sqrt{B_1^2 + B_2^2} \sin 2\phi_3 - 2\sqrt{B_3^2 + B_4^2} \sin(\phi_4 - \phi_3) \right] \quad (16)$$

and, the efficiency for the subharmonic parametric resonance is

$$\eta_{SPR} = \frac{E[P_{out}]_{SPR}}{E[P_{in}]_{SPR}} = \frac{4\beta(B_5^2 + B_6^2 + B_7^2 + B_8^2)}{\Omega f \sqrt{B_1^2 + B_2^2} \left[\sqrt{B_1^2 + B_2^2} \sin 2\phi_3 - 2\sqrt{B_3^2 + B_4^2} \sin(\phi_4 - \phi_3) \right]} \quad (17)$$

where the corresponding phase angles are

$$\phi_3 = \arctan\left(-\frac{B_2}{B_1}\right), \phi_4 = \arctan\left(-\frac{B_4}{B_3}\right) \quad (18)$$

Note that the first term in Eq. (16) is the contribution of the first-order subharmonic, the primary source of net power generation, whereas the second term in Eq. (16) is the contribution of the third-order subharmonic which also represents the net power inflow from the outside excitation to the energy harvesting system.

Considering Eq. (13) and Eq. (16), and combining with the evolution diagrams of the phase angle and the phase difference demonstrated in Figs. 9-13, we conclude that, for both the primary parametric resonance and the subharmonic parametric resonance, parametric excitation does positive work over a whole cycle acting upon the higher-order harmonic motion induced by nonlinearity in the mechanical system, which is benefit to the energy harvesting. However, for the directly excited nonlinear energy harvesters concerned by most researchers, as one kind of forced excitation, the work done by a harmonic force acting upon the higher-order harmonic motion of a different frequency from the force is zero during a whole cycle [50], which indicates that the nonlinear harmonics have no substantial benefit to the improvement of input power. It is worth pointing out that, generally speaking, maximizing the input power is a feasible way to enhance the output power. It is preliminarily revealed that the parametrically excited nonlinear energy harvesters are more valuable to develop than the directly excited ones if the output power as a leading performance metric is considered.

As shown in Figs. 9-13, the frequency responses of input power, output power and efficiency obtained are now examined. In addition, the corresponding frequency responses of phase illustrated furnish the basic dynamical information involving the primary harmonic and the secondary harmonic. Two parametric resonance regimes are observed, namely, the relatively narrow primary parametric resonance regime and the relatively wide subharmonic parametric resonance regime. A common characteristic in the two resonance regimes is that the output power is mainly determined by the input power, which is depending on the frequency and amplitude of the parametric excitation and also the phase information of the response, and as the excitation frequency is increased, the input power and the output power are both enhanced, that can be confirmed by the increased sine value of the phase angle and phase difference. Special features in the two resonance regimes are revealed in details.

Figure 9 shows that the variation of the input power, the output power, the efficiency and the phase with respect to the parametric excitation frequency Ω for three different nonlinearities. For both the primary parametric resonance and subharmonic parametric reso-

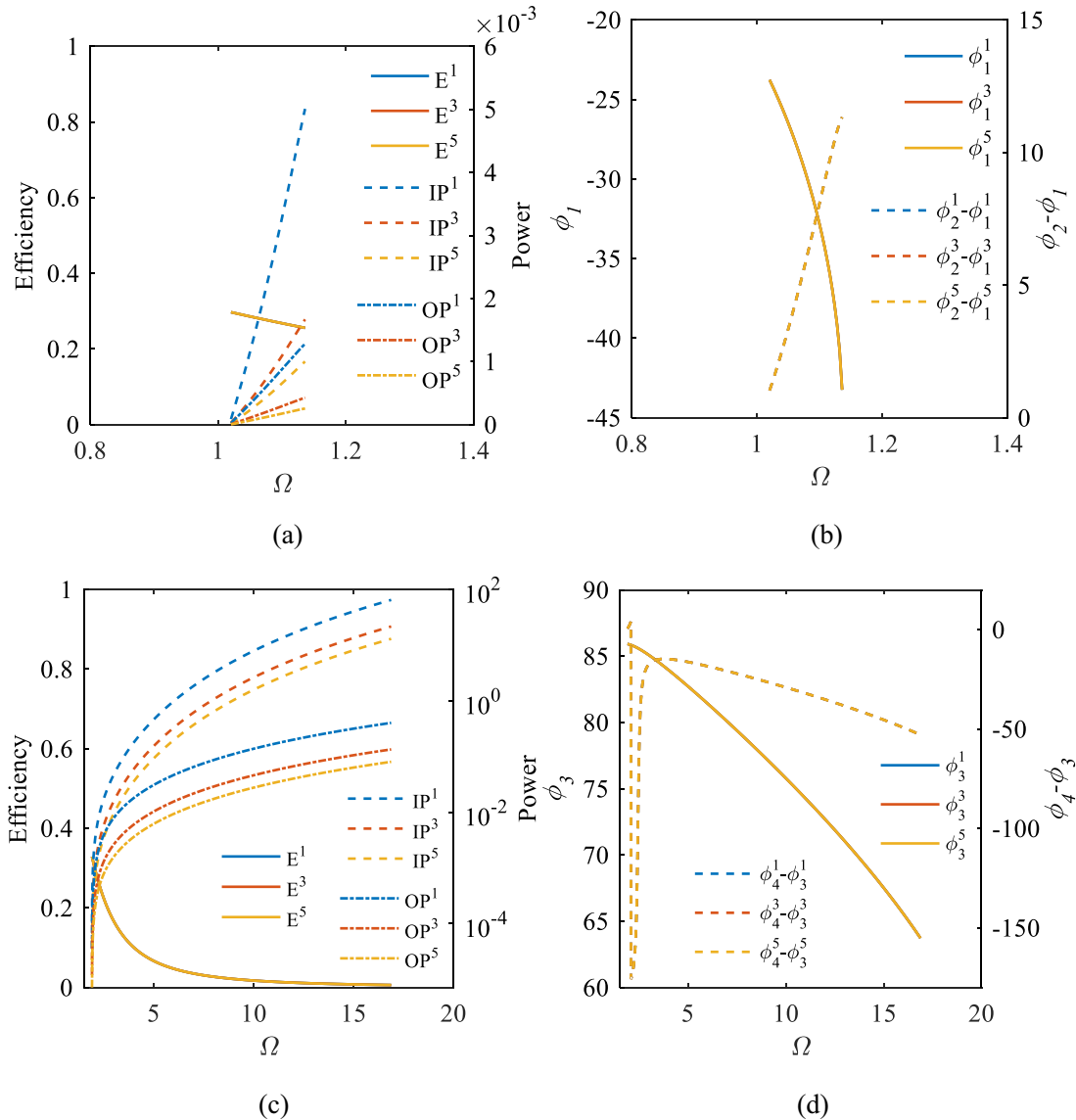


Fig. 9. Variation of input power (IP), output power (OP) and efficiency (E) with Ω for primary parametric resonance (a) and subharmonic parametric resonance (c) with different α ; Variation of phase (left label) and phase difference (right label) with Ω for primary parametric resonance (b) and subharmonic parametric resonance (d) with different α . $f = 0.4, \beta = 0.1, \mu = 0.02, \chi = 0.3, \alpha = 1$ ($E^1, IP^1, OP^1, \phi_1^1$), $\alpha = 3$ ($E^3, IP^3, OP^3, \phi_1^3$), $\alpha = 5$ ($E^5, IP^5, OP^5, \phi_1^5$).

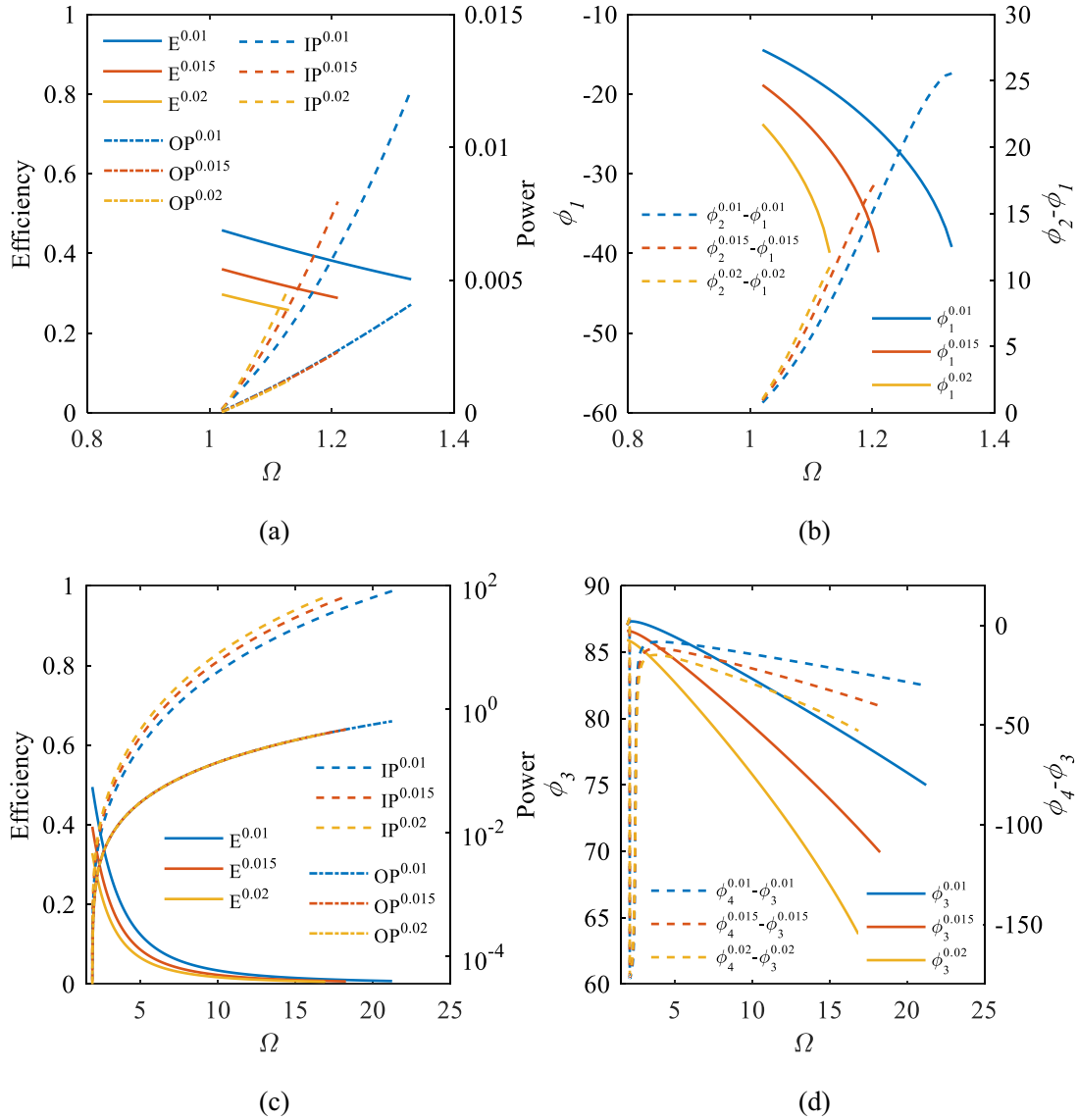


Fig. 10. Variation of input power (IP), output power (OP) and efficiency (E) with Ω for primary parametric resonance (a) and subharmonic parametric resonance (c) with different μ ; Variation of phase (left label) and phase difference (right label) with Ω for primary parametric resonance (b) and subharmonic parametric resonance (d) with different μ . $f = 0.4$, $\beta = 0.1$, $\alpha = 1$, $\chi = 0.3$, $\mu = 0.01$ ($E^{0.01}$, $IP^{0.01}$, $OP^{0.01}$, $\phi_1^{0.01}$), $\mu = 0.015$ ($E^{0.015}$, $IP^{0.015}$, $OP^{0.015}$, $\phi_1^{0.015}$), $\mu = 0.02$ ($E^{0.02}$, $IP^{0.02}$, $OP^{0.02}$, $\phi_1^{0.02}$).

nance, it is evident that, the input power and the output power is proportional to the excitation frequency, respectively, while the efficiency is inversely proportional to the excitation frequency. It can be explained that the higher the excitation frequency is, the more dissipation induced from the mechanical damping the vibratory energy harvester behaves, thus, it leads to a bigger difference between the input power and the output power, and consequently, a decreasing trend with respect to the excitation frequency. Unlike the scenario of directly excited energy harvesters in which both the input power and output power peak at resonance and plunge once excitation frequency deviates from resonance [49], as shown in Fig. 9(b) and Fig. 9(d), no “phase transition” occurs in both the primary and the subharmonic parametric resonance regimes for the primary harmonic motion. However, for the secondary harmonic motion in the subharmonic parametric resonance regime, “phase transition” arises within a narrow band. The term “phase transition” in this investigation refers to a phase change of π of the displacement amplitude of harmonic components. This intriguing feature of the frequency response of phase

differences may result in a sudden change of the frequency response of the input power and efficiency. However, such phenomenon cannot be evidently observed due to the relatively weak secondary harmonic response in the low frequency region of parametric resonance band. It is worth recalling that, for the directly excited energy harvesters, due to the additional damping and stiffness effects of the electrical system on the mechanical system [54], the resonance state corresponds to a phase difference between the dynamical response and the forced excitation, which is close but not equal to 90° [49]. However, a completely different law phase difference evolution appears, for the parametrically excited energy harvesters. Note that, the efficiency is independent to the nonlinearity level, resulting from the proportional amplification effect between the input power and the output power with respect to the excitation frequency, and the independence of the phase with respect to the nonlinearity level. Moreover, the bandwidth of the input power, the output power and the efficiency is still independent with the nonlinearity level, respectively, due to the inde-

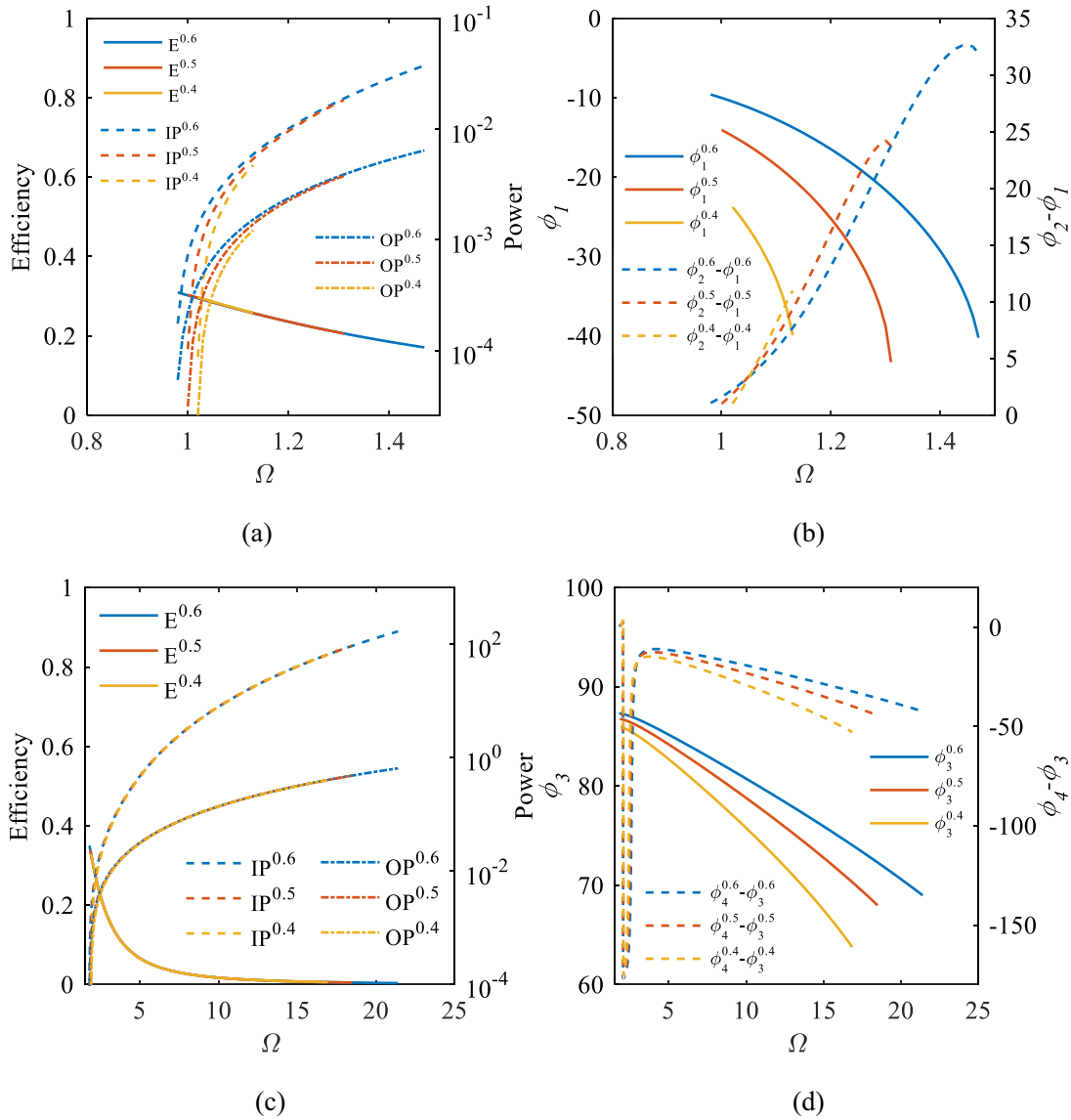


Fig. 11. Variation of input power (IP), output power (OP) and efficiency (E) with Ω for primary parametric resonance (a) and subharmonic parametric resonance (c) with different f ; Variation of phase (left label) and phase difference (right label) with Ω for primary parametric resonance (b) and subharmonic parametric resonance (d) with different f . $\mu = 0.02, \beta = 0.1, \alpha = 1, \chi = 0.3, f = 0.6$ ($E^{0.6}, IP^{0.6}, OP^{0.6}, \phi_1^{0.6}, \phi_2^{0.6} - \phi_1^{0.6}$), $f = 0.5$ ($E^{0.5}, IP^{0.5}, OP^{0.5}, \phi_1^{0.5}, \phi_2^{0.5} - \phi_1^{0.5}$), $f = 0.4$ ($E^{0.4}, IP^{0.4}, OP^{0.4}, \phi_1^{0.4}, \phi_2^{0.4} - \phi_1^{0.4}$).

pendence of the bandwidth of phase with respect to the nonlinearity level.

Figure 10 depicts the variation of the input power, the output power, the efficiency and the phase with respect to Ω for three different mechanical damping. It is clearly seen that the mechanical damping has quite an influence on the input power, the output power and the efficiency. Specifically, as increasing the mechanical damping, the bandwidth of input power, output power and efficiency shrink significantly. Note that, the variation of the mechanical damping does not affect the starting point of resonance band, but the terminal point. Although the smaller the mechanical damping is, the lower the input power generate, but because the output power appears to be not obviously influenced when excitation frequency is fixed, the efficiency increases as the mechanical damping is decreased. In other words, reducing mechanical damping not only expands the operation bandwidth, but also improves the efficiency.

On the other hand, increasing the amplitude of parametric excitation also significantly expands the bandwidth of input power, output power and efficiency, not only pushing forward the starting point of

resonance band, but also pushing back the terminal point, see Fig. 11. For the scenario of primary parametric resonance, although the variation of the excitation amplitude substantially influences the input power and output power, the efficiency seems to be unchanged when the excitation frequency is fixed. This results from the proportional amplification effect involving the input power and the output power with respect to the excitation frequency when the mechanical damping is maintained constant. However, for the scenario of subharmonic parametric resonance, the input power, the output power and the efficiency appear not to be affected by the excitation amplitude when the excitation frequency is fixed.

Figure 12 illustrates the variation of the input power, the output power, the efficiency and the phase with respect to Ω for three different time constant. For the scenario of the primary parametric resonance, as the time constant is increased from the approximate open-circuit case ($\beta = 0.001$), the input power increases gradually, and the output power significantly increases, hence, the efficiency increases considerably. Meanwhile, the bandwidth shrinks until the resonance band vanishes. Therefore, evaluating the performance of

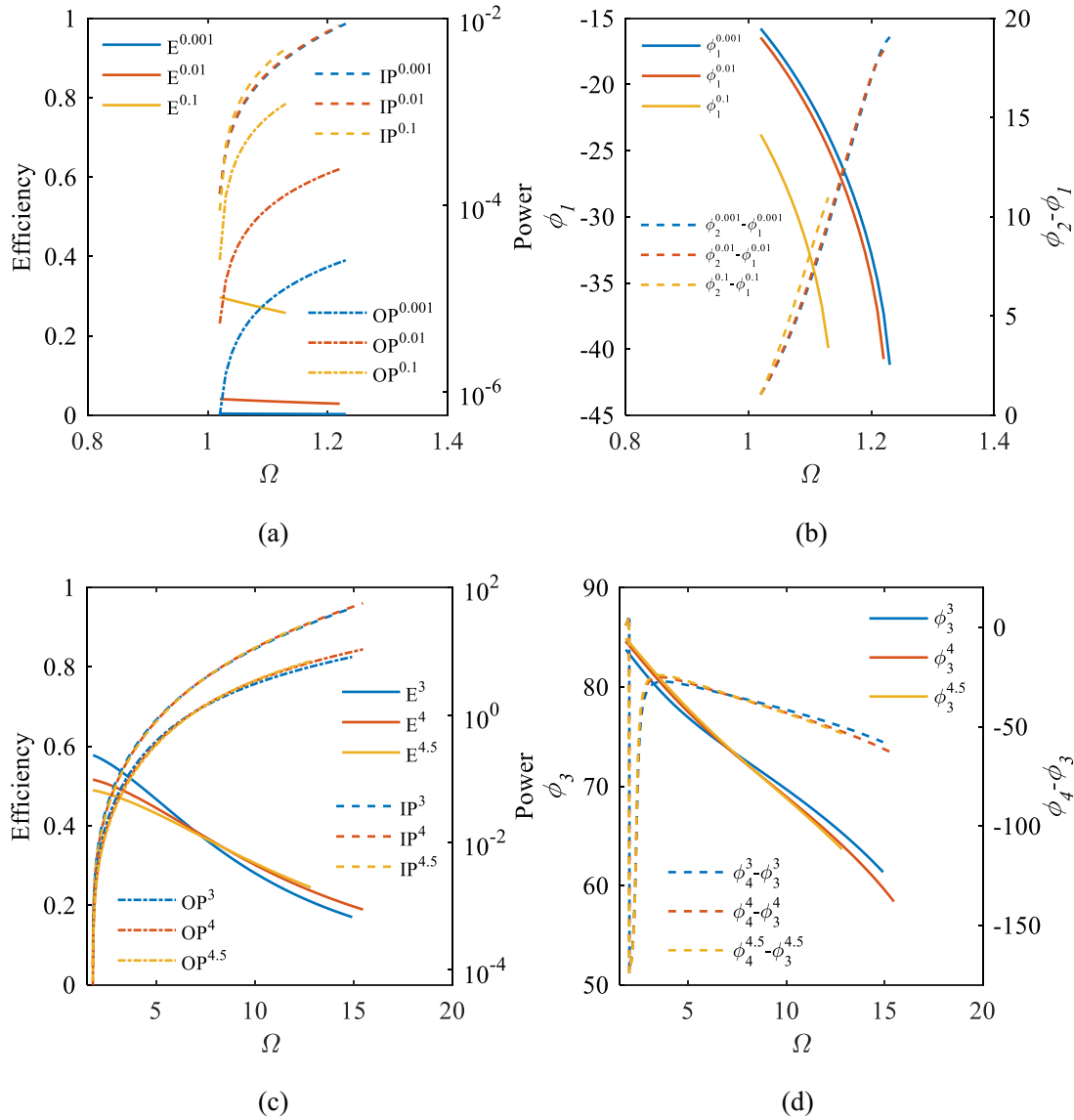


Fig. 12. Variation of input power (IP), output power (OP) and efficiency (E) with Ω for primary parametric resonance (a) and subharmonic parametric resonance (c) with different β ; Variation of phase (left label) and phase difference (right label) with Ω for primary parametric resonance (b) and subharmonic parametric resonance (d) with different β . $\mu = 0.02, f = 0.4, \alpha = 1, \chi = 0.3, \beta = 0.001$ ($E^{0.001}, IP^{0.001}, OP^{0.001}, \phi_1^{0.001}$), $\beta = 0.01$ ($E^{0.01}, IP^{0.01}, OP^{0.01}, \phi_1^{0.01}$), $\beta = 0.1$ ($E^{0.1}, IP^{0.1}, OP^{0.1}, \phi_1^{0.1}$), $\beta = 3$ ($E^3, IP^3, OP^3, \phi_3^3$), $\beta = 4$ ($E^4, IP^4, OP^4, \phi_4^4$), $\beta = 4.5$ ($E^{4.5}, IP^{4.5}, OP^{4.5}, \phi_4^{4.5}$).

vibratory energy harvesters needs comprehensive consideration. For the scenario of the subharmonic parametric resonance, a transition point exists within a certain parameter range. Specifically, when the excitation frequency is lower than the transition frequency, as the time constant is increased, the input power, the output power and the efficiency are slightly attenuated. But, when the excitation frequency is higher than the transition frequency, the input power, the output power and the efficiency are then slightly enhanced. If we only focus on the performance near the terminal point of resonance band, then, $\beta = 4$ can be regarded as an optimal time constant. These features inspire researchers to subtly select a time constant in order to obtain a better performance. Note that the performance of primary parametric resonance is more sensitive to the increased time constant than that of the subharmonic resonance, and the parametric resonance will settle down as further increasing time constant.

The influence of electromechanical coupling on the frequency response of input power, output power, efficiency and phase is shown

in Fig. 13. For both primary parametric resonance and subharmonic parametric resonance, maximum output power exists as the electromechanical coupling is varied. The reason of the existence of optimal electromechanical coupling could be essentially explained from the perspective of energy balance. In fact, Fig. 13(a) and Fig. 13(c) show that, as expected, the higher the electromechanical coupling is, the higher energy conversion efficiency from the mechanical system to the electrical system is, which but leads to a weaker mechanical response and then input power reduction and also corresponding resonance bandwidth shrink. The decreased input power will be further detrimental to the output power generation. Consequently, there is no need to constantly improve piezoelectric materials' electromechanical conversion factor, if one mainly concerns high output power generation. For the primary parametric resonance, the output power peaks at the optimal value $\chi = 0.3$ and then drop evidently. For the subharmonic parametric resonance, the output power reaches the maximum at the optimal value $\chi = 0.9$ and then drop. Further increasing the

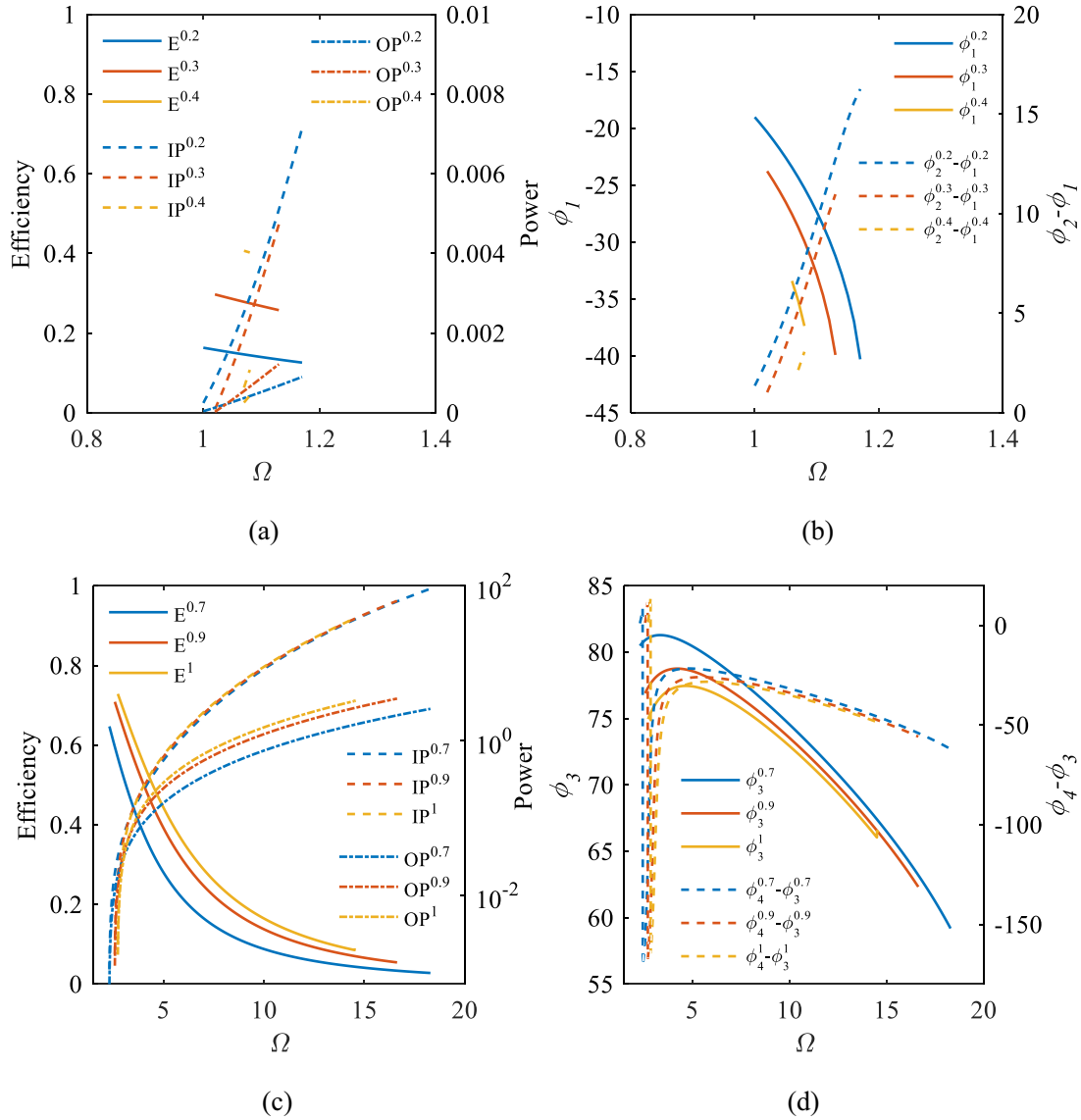


Fig. 13. Variation of input power (IP), output power (OP) and efficiency (E) with Ω for primary parametric resonance (a) and subharmonic parametric resonance (c) with different χ ; Variation of phase (left label) and phase difference (right label) with Ω for primary parametric resonance (b) and subharmonic parametric resonance (d) with different χ . $\mu = 0.02, f = 0.4, \alpha = 1, \beta = 0.1, \chi = 0.2$ ($E^{0.2}, IP^{0.2}, OP^{0.2}, \phi_1^{0.2}$), $\chi = 0.3$ ($E^{0.3}, IP^{0.3}, OP^{0.3}, \phi_1^{0.3}$), $\chi = 0.4$ ($E^{0.4}, IP^{0.4}, OP^{0.4}, \phi_1^{0.4}$), $\chi = 0.7$ ($E^{0.7}, IP^{0.7}, OP^{0.7}, \phi_1^{0.7}$), $\chi = 0.9$ ($E^{0.9}, IP^{0.9}, OP^{0.9}, \phi_1^{0.9}$), $\chi = 1$ ($E^1, IP^1, OP^1, \phi_1^1$).

electromechanical coupling will result in sharp shrinkage of the bandwidth near the region where the optimal electromechanical coupling is located.

5. Performance comparisons with directly excited energy harvesting systems

In this section, by comparing directly excited linear energy harvesting system (DEL), directly excited nonlinear energy harvesting system (DEN) and parametrically excited nonlinear energy harvesting system (PEN), the broad band and high efficiency advantage of parametrically excited scenario is first confirmed, as shown in Fig. 14 and the features of instantaneous input power, dissipative power and output power are then revealed, see Fig. 15. Herein, comparisons between DEN and PEN are implemented via the same electromechanical coupling system but excited by different directional harmonic vibrations, and the results of DEL, as a benchmark, are achieved by setting the nonlinearity to be zero.

The frequency response diagrams of averaged output power (Fig. 14(a) and Fig. 14(c)) demonstrate that, as the excitation amplitude is increased, for DEN under primary resonance, although the effective bandwidth slightly increases, comparing with DEL, the peak difference between them increases significantly. That, to a certain extent, limits the potential applications of DEN. In other words, one should balance the effect of bandwidth increase and that of relative peak reduction when employing DEN. However, it is inspiring to see that, for PEN under subharmonic resonance, both the bandwidth and the peak of averaged output power increase significantly. It is worth noting that, for extremely small excitation amplitude, DEN will gain advantages over PEN because the steady-state response may not even be excited for the nonlinear energy harvesting system under weak parametric excitation. For energy conversion efficiency (Fig. 14(b) and (d)), PEN is always superior to DEN within the subharmonic resonance region, regardless of the excitation amplitude.

Based on the energy balance equation, we conclude that the ultimate goal of vibratory energy harvesting is to minimize damping dis-

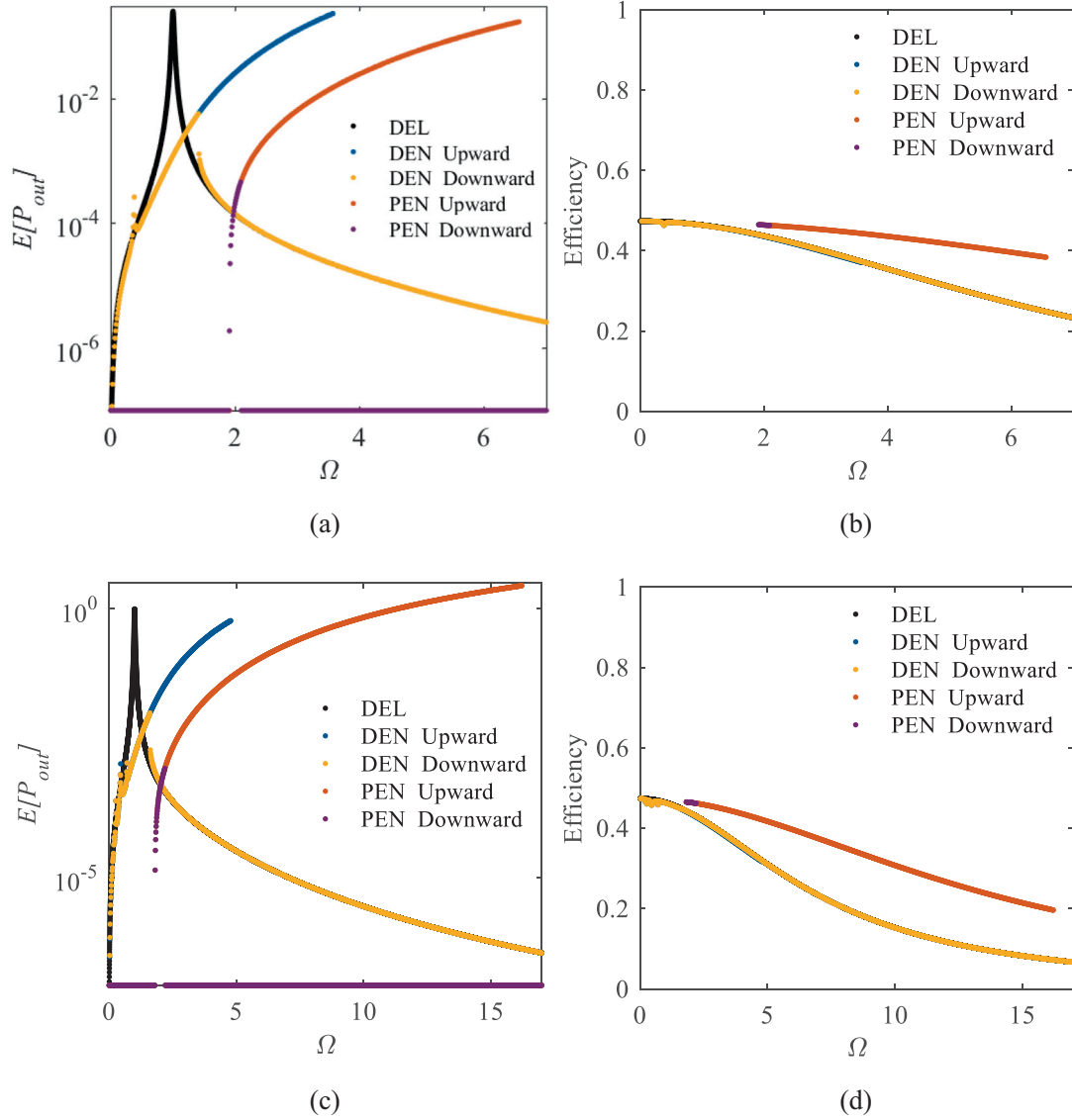


Fig. 14. Variation of output power (a) and efficiency (b) with Ω for $f = 0.2$; Variation of output power (c) and efficiency (d) with Ω for $f = 0.4$. $\mu = 0.02$, $\alpha = 5$, $\beta = 5$, $\chi = 0.3$.

sipation and maximize power input. It is easy to minimize damping dissipation by employing the structural material with low damping factor. Maximizing power input, actually requiring the excitation to do positive work to the energy harvesting system in each cycle, such supreme on-resonance state exists in DEL, DEN and PEN, as shown in Fig. 15(a), (c) and (e), respectively. However, when the excitation frequency of the vibration source is far from the supreme on-resonance frequency, it is inevitable to do negative work for a certain period in each cycle, that is, some energy flows back the vibration source, see Fig. 15(b), (d) and (f). These features are universal for vibration-based energy harvesting systems, which are the essential characteristics that distinguishes it from photovoltaic power generation.

6. Conclusions

In this paper, we analyze the performance of a parametrically excited piezoelectric energy harvester as viewed from energy transformation in mechanic-electronics. New dimensionless transformations capturing

the essence of two-way electromechanical coupling are employed to obtain a dimensionless dynamical system. Based on it, two types of observable resonances, namely, the primary parametric resonance with narrow bandwidth and the subharmonic parametric resonance with wide bandwidth, are investigated by using the harmonic balance method and the energy balance equation. The variation law of the mean-square voltage, the input power, the output power, the energy conversion efficiency, the phase angle and the phase difference with dimensionless parameters is first revealed in details and the optimal parameter values in which the performance is maximized are discussed. The main results obtained can be briefly summarized as follows:

(1) For both two types of parametric resonance, the performance of vibratory energy harvesters stems from the input power which is proportional to the frequency and amplitude of the parametric excitation, and directly related to the amplitude, phase angle and phase difference of the response.

(2) The amplitude, phase angle and phase difference of the response are essentially depending on the comprehensive effects between the parametric excitation and the dimensionless system parameters.

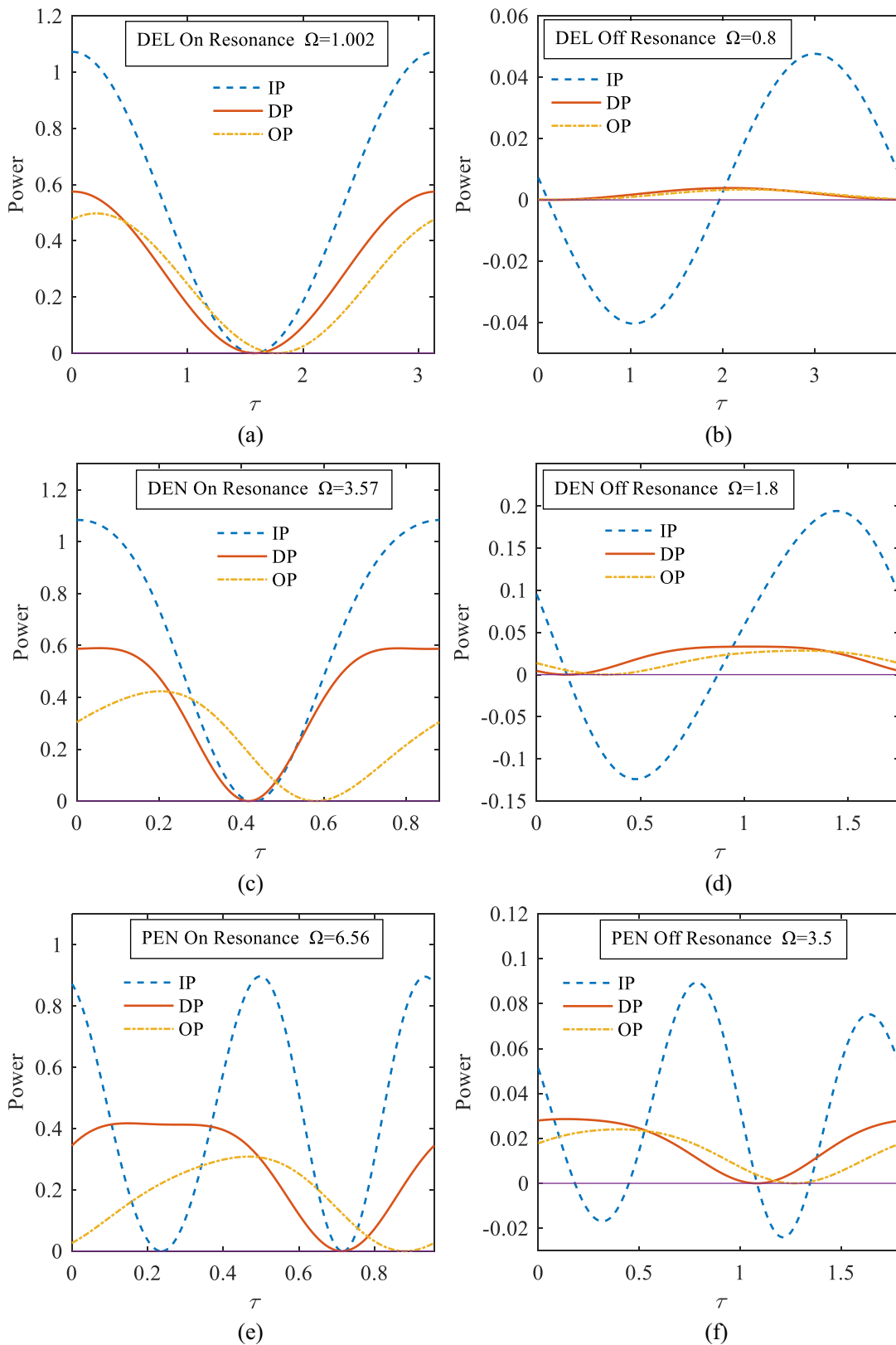


Fig. 15. Instantaneous input power (IP), dissipative power (DP), and output power (OP) in each cycle for directly excited linear energy harvesting system (a) and (b), directly excited nonlinear energy harvesting system (c) and (d), and parametrically excited nonlinear energy harvesting system (e) and (f). $\mu = 0.02, f = 0.2, \alpha = 5, \beta = 5, \chi = 0.3$.

(3) Due to the broadband characteristics, the subharmonic parametric resonance pumps much more power input and output than the primary parametric resonance.

(4) For the directly excited nonlinear energy harvesters, broadband and high output power cannot be achieved simultaneously. However, for the parametrically excited nonlinear energy harvesters, the wide bandwidth results in considerable power output.

(5) For the directly excited nonlinear energy harvesters, broadband performance requires strong nonlinearity. However, the bandwidth of the parametrically excited nonlinear energy harvesters is independent to the nonlinearity level. Moreover, weaker nonlinearity leads to stronger power input and output.

(6) For both the directly excited nonlinear energy harvesters and the parametrically excited nonlinear energy harvesters, supreme on-resonance state exists, where maximized power input can be achieved via the excitation doing positive work to the energy harvesting system in each cycle.

(7) For the parametrically excited nonlinear energy harvesters, parametric excitation does positive work over a whole cycle acting upon the higher-order harmonic motion induced by nonlinearity in the mechanical system, which is benefit to the energy harvesting. However, for the directly excited nonlinear energy harvesters, the work done by a harmonic force acting upon the higher-order harmonic motion is zero during a whole cycle, revealing that the nonlinear harmonics have no substantial benefit to the enhancement of input power and output power.

(8) Within the effective resonance band, the energy conversion efficiency of the same energy harvesters under parametric excitation is higher than that under direct excitation.

(9) The parametrically excited nonlinear energy harvesters under subharmonic parametric resonance are more suitable for the weakly nonlinear electromechanical systems subjected to the relatively strong excitation. Such subharmonic broadband response feature also has potential applications in designing advanced mechanical filters and converters.

7. Data Availability

The data that support the findings of this study are available on request from the corresponding author.

CRedit authorship contribution statement

Tianjun Yu: Conceptualization, Investigation, Visualization, Writing – original draft. **Sha Zhou:** Methodology, Supervision, Validation.

Declaration of Competing Interest

The authors declare that they have no known competing financial interests or personal relationships that could have appeared to influence the work reported in this paper.

Acknowledgements

The authors gratefully acknowledge that the financial support from the National Natural Science Foundation of China (11802266, 11802016), the National Key R&D Program of China (2018YFC0809400) and the China Postdoctoral Science Foundation (2018M631349).

References

- [1] Khadem SE, Shahgholi M, Hosseini SAA. Two-mode combination resonances of an in-extensional rotating shaft with large amplitude. *Nonlinear Dyn* 2011;65(3):217–33.
- [2] Yabuno H, Kashimura T, Inoue T, Ishida Y. Nonlinear normal modes and primary resonance of horizontally supported Jeffcott rotor. *Nonlinear Dyn* 2011;66(3):377–87.
- [3] Yamamoto T, Ishida Y. *Linear and nonlinear Rotordynamics: A modern treatment with applications*. Weinheim: Wiley-VCH; 2012.
- [4] Chávez JP, Wiercigroch M. Bifurcation analysis of periodic orbits of a non-smooth Jeffcott rotor model. *Comm Nonlinear Sci Numer Simul* 2013;18:2571–80.
- [5] Ghayesh MH, Farokhi H, Alici G. Size-dependent performance of microgyroscopes. *Int J Eng Sci* 2016;100:99–111.
- [6] Yu TJ, Zhou S, Zhang W, Yang XD. Multi-pulse chaotic dynamics of an unbalanced Jeffcott rotor with gravity effect. *Nonlinear Dyn* 2017;87(1):647–64.
- [7] Paidoussis MP. *Fluid-structure interactions: slender structures and axial flow*. San Diego: Academic Press; 1998.
- [8] Panda LN, Kar RC. Nonlinear dynamics of a pipe conveying pulsating fluid with parametric and internal resonances. *Nonlinear Dyn* 2007;49(1-2):9–30.
- [9] Ghayesh MH, Paidoussis MP, Amabili M. Nonlinear dynamics of cantilevered extensible pipes conveying fluid. *J Sound Vib*. 2013;332(24):6405–18.
- [10] Tan X, Ding H, Chen L-Q. Nonlinear frequencies and forced responses of pipes conveying fluid via a coupled Timoshenko model. *J. Sound Vib* 2019;455:241–55.
- [11] Singh K, Michelin S, Langre E. The effect of non-uniform damping on flutter in axial flow and energy-harvesting strategies. *Proc R Soc A* 2012;468:3620–35.
- [12] Zhang LW, Song ZG, Liew KM. Computation of aerothermoelastic properties and active flutter control of CNT reinforced functionally graded composite panels in supersonic airflow. *Comput Method Appl Mech* 2016;300:427–41.
- [13] Yu TJ, Zhou S, Yang XD, Zhang W. Homoclinic orbits and chaos of a supercritical composite panel with free-layer damping treatment in subsonic flow. *Compos Struct* 2017;159:288–98.
- [14] Yu TJ, Zhou S, Yang XD, Zhang W. Global dynamics of composite panels with free-layer damping treatment in subsonic flow. *Compos Struct* 2017;168:247–58.
- [15] Yang Z, Huang R, Liu H, Zhao Y, Hu H. An improved nonlinear reduced-order modeling for transonic aeroelastic systems. *J Fluid Struct* 2020;94:102926. <https://doi.org/10.1016/j.jfluidstruct.2020.102926>.
- [16] Zurbuchen A, Pfenniger A, Stahel A, Stoeck CT, Vandenberghe S, Koch VM, et al. Energy harvesting from the beating heart by a mass imbalance oscillation generator. *Ann Biomed Eng* 2013;41:131–41.
- [17] Pfenniger A, Wichramaratna LN, Vogel R, Koch VM. Design and realization of an energy harvester using pulsating arterial pressure. *Med Eng Phys* 2013;35:1256–65.
- [18] Zhang YY, Lu BW, Lü CF, Feng X. Theory of energy harvesting from heartbeat including the effects of pleural cavity and respiration. *Proc R Soc A* 2017;473:20170615.
- [19] Ali F, Raza W, Li X, Gul H, Kim K-H. Piezoelectric energy harvesters for biomedical applications. *Nano Energy* 2019;57:879–902.
- [20] Li JF, Zhou XM, Huang GL, Hu GK. Acoustic metamaterials capable of both sound insulation and energy harvesting. *Smart Mater Struct* 2016;25:045013.
- [21] Hu GB, Tang LH, Banerjee A, Das R. Metastucture with piezoelectric element for simultaneous vibration suppression and energy harvesting. *ASME J Vib Acoust* 2017;139:011012.
- [22] Hu GB, Tang LH, Das R. Internally coupled metamaterial beam for simultaneous vibration suppression and low frequency energy harvesting. *J Appl Phys* 2018;123:055107.
- [23] Zhang YW, Su C, Ni ZY, Zang J, Chen LQ. A multifunctional lattice sandwich structure with energy harvesting and nonlinear vibration control. *Compos Struct* 2019;221:110875.
- [24] Daqaq MF, Masana R, Erturk A, Quinn DD. On the role of nonlinearities in vibratory energy harvesting: a critical review and discussion. *Appl Mech Rev* 2014;66:040801.
- [25] Tran N, Ghayesh MH, Arjomandi M. Ambient vibration energy harvesters: a review on nonlinear techniques for performance enhancement. *Int J Eng Sci* 2018;127:162–85.
- [26] Mann BP, Sims ND. Energy harvesting from the nonlinear oscillations of magnetic levitation. *J Sound Vib* 2008;319:515–30.
- [27] Stanton SC, McGehee CC, Mann BP. Nonlinear dynamics for broadband energy harvesting: investigation of a bistable piezoelectric inertial generator. *Phys D* 2010;239:640–53.
- [28] Ramlan R, Brennan MJ, Mace BR, Kovacic I. Potential benefits of a non-linear stiffness in an energy harvesting device. *Nonlinear Dyn* 2010;59(4):545–58.
- [29] Quinn DD, Triplett AL, Bergman LA, Vakakis AF. Comparing linear and essentially nonlinear vibration-based energy harvesting. *ASME J Vib Acoust* 2011;133:011001.
- [30] Wei CF, Jing XJ. Vibrational energy harvesting by exploring structural benefits and nonlinear characteristics. *Commun Nonlinear Sci Numer Simul* 2017;48:288–306.
- [31] Qian F, Zhou SX, Zuo L. Approximate solutions and their stability of a broadband piezoelectric energy harvester with a tunable potential function. *Commun Nonlinear Sci Numer Simul* 2020;80:104984.
- [32] Erturk A, Inman DJ. A distributed parameter electromechanical model for cantilevered piezoelectric harvesters. *ASME J Vib Acoust* 2008;130:041002.
- [33] Masana R, Daqaq MF. Relative performance of a vibratory energy harvester in mono- and bi-stable potentials. *J Sound Vib* 2011;330(24):6036–52.
- [34] Lan CB, Qin WY, Deng WZ. Energy harvesting by dynamic instability and internal resonance for piezoelectric beam. *Appl Phys Lett* 2015;107:093902.
- [35] Rezaei M, Khadem SE, Firoozy P. Broadband and tunable PZT energy harvesting utilizing local nonlinearity and tip mass effects. *Int J Eng Sci* 2017;118:1–15.
- [36] Xiao S, Jin Y. Response analysis of the piezoelectric energy harvester under correlated white noise. *Nonlinear Dyn* 2017;90(3):2069–82.

- [37] Yang ZB, Wang YQ, Zuo L, Zu J. Introducing arc-shaped piezoelectric elements into energy harvesters. *Energ Convers Manage* 2017;148:260–6.
- [38] Zhou SX, Zuo L. Nonlinear dynamic analysis of asymmetric tristable energy harvesters for enhanced energy harvesting. *Commun Nonlinear Sci Numer Simul* 2018;61:271–84.
- [39] Banerjee S, Roy S. A Timoshenko like model for piezoelectric energy harvester with shear mode. *Compos Struct* 2018;204:677–88.
- [40] Wang B, Luo XW, Liu YZ, Yang ZB. Thickness-variable composite beams for vibration energy harvesting. *Compos Struct* 2020;244:112232.
- [41] Sebald G, Kuwano H, Guyomar D, Ducharme B. Simulation of a Duffing oscillator for broadband piezoelectric energy harvesting. *Smart Mater Struct* 2011;20:075022.
- [42] Daqaq MF, Stabler C, Qaroush Y, Seuaciuc-Osório T. Investigation of power harvesting via parametric excitations. *J Intel Mat Syst Str* 2009;20:545–57.
- [43] Ma TW, Zhang H, Xu NS. A novel parametrically excited non-linear energy harvester. *Mech Syst Signal Pr* 2012;28:323–32.
- [44] Abdelkefi A, Nayfeh AH, Hajj MR. Global nonlinear distributed-parameter model of parametrically excited piezoelectric energy harvesters. *Nonlinear Dyn* 2012;67(2):1147–60.
- [45] Jia Y, Yan JZ, Soga K, Seshia AA. A parametrically excited vibration energy harvester. *J Intel Mat Syst Str* 2014;25:278–89.
- [46] Panyam M, Daqaq MF, Emam SA. Exploiting the subharmonic parametric resonances of a buckled beam for vibratory energy harvesting. *Meccanica* 2018;53(14):3545–64.
- [47] Garg A, Dwivedy SK. Piezoelectric energy harvester under parametric excitation: a theoretical and experimental investigation. *J Intel Mat Syst Str* 2020;31:612–31.
- [48] Ghayesh MH, Farokhi H. Nonlinear broadband performance of energy harvesters. *Int J Eng Sci* 2020;147:103202.
- [49] Yang ZB, Erturk A, Zu J. On the efficiency of piezoelectric energy harvesters. *Extreme Mech Lett* 2017;15:26–37.
- [50] Den Hartog JP. *Mechanical vibrations*. New York: Dover Publications; 1985.
- [51] Zhou S, Yu TJ. Performance comparisons of piezoelectric energy harvesters under different stochastic noises. *AIP Adv* 2020;10(3):035033. <https://doi.org/10.1063/1.5141478>.
- [52] Yu TJ, Zhou S. Performance investigations of nonlinear piezoelectric energy harvesters with a resonant circuit under white Gaussian noises. *Nonlinear Dyn* 2021;103(1):183–96.
- [53] Nayfeh AH, Mook DT, editors. *Nonlinear Oscillations*. Wiley; 1995.
- [54] Karami MA, Inman DJ. Equivalent damping and frequency change for linear and nonlinear hybrid vibrational energy harvesting systems. *J Sound Vib* 2011;330(23):5583–97.